Heliyon 9 (2023) e18846

Contents lists available at ScienceDirect

Heliyon

journal homepage: www.cell.com/heliyon

Time-series analyses of land surface temperature changes with Google Earth Engine in a mountainous region

Cátia Rodrigues de Almeida [a,b,c], Nuno Garcia [d], João C. Campos [d], João Alírio [a], Salvador Arenas-Castro [e], Artur Gonçalves [c,f], Neftalí Sillero [d], Ana Cláudia Teodoro [a,b,*]

[a] Department of Geosciences, Environment and Land Planning, University of Porto, Rua Campo Alegre, 687, 4169-007, Porto, Portugal
[b] Earth Sciences Institute (ICT), Pole of the FCUP, University of Porto, 4169-007, Porto, Portugal
[c] Centro de Investigação de Montanha (CIMO), Instituto Politécnico de Bragança (IPB), Campus de Santa Apolónia, 5300-253 Bragança, Portugal
[d] CICGE-Centro de Investigação em Ciências GeoEespaciais, Faculdade de Ciências da Universidade do Porto, Alameda do Monte da Virgem, 4430-146 Vila Nova de Gaia, Portugal
[e] Área de Ecología, Dpto. de Botánica, Ecología y Fisiología Vegetal, Facultad de Ciencias, Universidad de Córdoba, Campus de Rabanales, 14071, Córdoba, Spain
[f] Laboratório Associado para a Sustentabilidade e Tecnologia em Regiões de Montanha (SusTEC), Instituto Politécnico de Bragança, Campus de Santa Apolónia, 5300-253, Bragança, Portugal

ARTICLE INFO

Keywords:
Temperature seasonality analysis
Air temperature
MODIS data
Montesinho natural park statistical analysis
Vegetation indexes

ABSTRACT

Studying changes in temperature is fundamental for understanding its interactions with the environment and biodiversity. However, studies in mountainous areas are few, due to their complex formation and the difficulty of obtaining local data. We analysed changes in temperature over time in Montesinho Natural Park (MNP) (Bragança, Portugal), an important conservation area due to its high level of biodiversity. Specifically, we aimed to analyse: i) whether temperature increased in MNP over time, ii) what environmental factors influence the Land Surface Temperature (LST), and iii) whether vegetation is related to changes in temperature. We used annual summer and winter mean data acquired from the Moderate-Resolution Imaging Spectroradiometer (MODIS) datasets/products (e.g. LST, gathered at four different times: 11am, 1pm, 10pm and 2am, Enhance vegetation index - EVI, and Evapotranspiration - ET), available on the cloud-based platform Google Earth Engine between 2003 and 2021). We analysed the dynamics of the temporal trend patterns between the LST and local thermal data (from a weather station) by correlations; the trends in LST over time with the Mann-Kendall trend test; and the stability of hot spots and cold spots of LST with Local Statistics of Spatial Association (LISA) tests. The temporal trend patterns between LST and Air Temperature (T_{air}) data were very similar ($\rho > 0.7$). The temperature in the MNP remained stable over time during summer but increased during winter nights. The biophysical indices were strongly correlated with the summer LST at 11am and 1pm. The LISA results identified hot and cold zones that remained stable over time. The remote-sensed data proved to be efficient in measuring changes in temperature over time.

* Corresponding author. Department of Geosciences, Environment and Land Planning, University of Porto, Rua Campo Alegre, 687, 4169-007, Porto, Portugal.
E-mail address: amteodor@fc.up.pt (A.C. Teodoro).

https://doi.org/10.1016/j.heliyon.2023.e18846
Received 28 February 2023; Received in revised form 28 July 2023; Accepted 31 July 2023
Available online 1 August 2023

1. Introduction

Earth's temperature is influenced by several factors, such as: i) altitude and relief, which influence air temperature (the higher the altitude, the fewer the particles absorbing and diffusing solar radiation, resulting in lower temperatures) and act as natural barriers to the movement of air masses/prevalent wind patterns [1]; ii) sea and land structures, resulting in local variations, that can be opposed (dry and torrid heat on slopes exposed directly to the sun, occasional thermal inversion, particularly at night and in enclosed valleys [1]; iii) global wind patterns, that shift north or south according to the seasons [1,2]; iv) latitude and the angles of the sun rays, determined by the tilt of the Earth's axis, changing the angle of incidence of electromagnetic energy and altering the day duration at different altitudes; and v) anthropogenic effects on atmospheric and oceanic temperature [3].

The increase in temperature can influence the Earth's natural dynamics. Water vapour, evaporation rate, and changes in the hydrological cycle increase with atmospheric warming, raising the frequency of torrential rains [4]. Climate change is increasing the intensity and frequency of extreme heat events, namely at higher latitudes [5], and is also shifting the distributions of ecosystems, plants and animals, whose persistence is associated with climate rhythm and stability [6,7].

Several studies have analysed the influence of environmental characteristics (e.g. topography, Land Use Land Cover - LULC, the presence of vegetation and its influence on the local climate) in the thermal behaviour and its possible impacts on the health and welfare of human populations and Earth's biomes and, in some cases, to guide strategic decision-making aimed at mitigating its impacts [8–10]. However, research studies analysing thermal changes in mountainous regions present a great complexity, due to the difficulty in separating the natural effects (temperature, precipitation, and radiation) from the anthropic ones [11]. In addition, the morphology and geological characteristics of mountainous areas create a high climatic variability in short periods of time, resulting in high daily and annual thermal amplitude, high inter-annual climatic variation, and extreme winter conditions, with the presence of snow in some months or during all-year [12,13]. There are several impacts associated with mountainous regions, among them: i) the melting of glaciers, which influences the availability of water resources for local human communities (for irrigation, wind energy production, and human consumption), as occurs in the Andes, the Himalayan Cordillera and the Alps [14,15]); ii) increase and intensity of extreme climate events, which can result in floods, droughts, and landslides [16]; iii) vulnerability of ecosystems to climate change, affecting animal and plant species that may not survive in their natural habitats, conditioning their migration to other regions [6,7,17,18]; and iv) increased risk of forest fires, both due to the increase in temperature, decrease in air humidity, and precipitation changes, reducing the amount of moisture available for vegetation [19].

Obtaining T_{air} from *in situ* meteorological stations in mountainous regions is difficult due to their low accessibility and distribution [20]. Remote Sensing (RS) is a valid alternative technique to analyse the changes in temperature of mountainous regions, as it provides empirical and effective indicators related to crucial environmental and ecological information at the site level [20]. Land Surface Temperature (LST) is a RS thermal product widely used in studies about the thermal behaviour of a site [21]. LST, differently from T_{air}, measures the thermal radiance emission from the land surface, which receives the incoming solar energy heating the ground [22]. LST is a good indicator of energy partitioning at the land surface-atmosphere boundary and is sensitive to changing surface conditions [22–25]. Thermal sensors operate in the atmospheric window (between 8 and 14 μm); the thermal sensors are cooled near 0 K and the observed target temperature is compared with internal reference temperatures (absolute radiation) [26]. LST is estimated from the radiometric temperature aggregate value contained in the sensor's field of view, estimated as emitted surface radiation (deduced in the atmospheric correction) or by inverse application of the Planck function, considering the effects of emissivity [22–24].

The most used thermal sensors are those onboard the satellites Landsat (starting with Landsat 4), with a temporal resolution of 16 days and spatial resolution resampled to 30 m (the Thematic Mapper (TM) sensor on board Landsat 4 and 5 obtain information at 120 m and the Thermal Infrared Sensor (TIRS) and Thermal Infrared Sensor-2 (TIRS 2) sensors on board Landsat 8 and 9, respectively, obtain information at 100 m); Terra/Aqua (MODIS - Moderate Resolution Imaging Spectrometer) with a spatial resolution of 1 km and temporal resolution of twice daily and Terra (ASTER - Advanced Spaceborne Thermal Emission and Reflectance Radiometer), with a temporal resolution of twice daily and spatial resolution of 90 m [21]. Other sensors are available with a higher temporal resolution, such as those onboard geostationary satellites (which observe the same point on Earth) and polar satellites that collect information from the same point at two times each day - one in an ascending and one in a descending orbit. The revisit time depends on the latitude. Examples of geostationary and polar satellites are the Spinning Enhanced Visible and InfraRed Imager (SEVIRI), with spatial resolution of 3 km, approximately [21,27] and the Geostationary Operational Environmental System (GOES), with spatial resolution of 4 km, approximately [21,28,29].

In view of the relevance of assessing how climate changes over time in mountainous regions, we selected as study area the Montesinho Natural Park (MNP) located in Bragança (Portugal), due to the following characteristics: i) a high vegetation diversity, allowing to analyse the influence of vegetation on local thermal behaviour; and ii) it has a local meteorological station that measures T_{air}, whose data can be used to analyse its relationship with LST data. Thus, our main objective is to analyse changes in LST over time (from 2003 to 2021) in the MNP. Specifically, we aimed to analyse: i) whether temperature increased in MNP over time; ii) what environmental factors influence the LST; and iii) whether vegetation is related to changes in temperature. We hypothesise that: (1) the temperature of MNP increased in the analysed period, due to climate change, (2) topography influences the LST, due to the presence of valleys and ridges in the study area; and (3) forests exerted a positive influence on temperature cooling in MNP. This is the first study, to our knowledge, analysing LST trends with an extensive 19-year time series collected at four different MODIS pass times and using other RS data (e.g. biophysical indices, topography). Notwithstanding, we also calculated the LST from the Landsat satellite series (namely 5, 7 and 8) and apply analytical methods to compare with the results obtained from MODIS, comparing them with another RS source with better spatial resolution. We obtained and processed the RS data in Google Earth Engine (GEE). We expect to further stimulate research on the effect of climate change in mountainous regions.

2. Materials and methods

2.1. Study area

The MNP, one of the largest protected areas in Portugal (41° 43′ 47″ to 41° 59′ 24″ N latitude and 6° 30′ 53″ to 7° 12′ 9″ W longitude), has 74224.89 ha (Fig. 1) [30–32] and an elevation range from 438 m to 1481 m above mean sea level (amsl). MNP hosts a high biodiversity, including priority habitats such as oak forests, meadows, grasslands, and bushlands with 1058 species of flora, 153 of nesting birds, 42 of mammals, 20 of reptiles and 13 of amphibians [32].

The average annual temperature varies between 8.5 °C and 12.8 °C. The average minimum and maximum annual temperatures range between 5 and 7 °C and 14 and 17 °C, respectively [32]. Due to the phenomenon of thermal inversion, which occurs mainly in the months of spring and winter (March to May, and December to February, respectively), the minimum temperatures in valley areas are often lower than those observed at higher altitudes [1,32,34]. In the eastern zones, the soil water deficit is recorded for a period of four months (June to September) and, in the central and western zones, for three months (July to September) [32]. The highest temperature values and the lowest precipitation levels occur in the eastern areas, because: i) greater exposure to sun and wind, due to its location in plateau areas and its predominant south-facing slopes, resulting in a hotter and drier climate; ii) the mountains located to the west, which makes the area less receptive to the rains coming from the Atlantic; iii) lower and less dense vegetation cover, which contributes to less moisture retention in the soil and greater solar exposure [31,32,35]. The opposite pattern is identified in the western areas (Montesinho and Coroa massifs) and surrounding areas.

The annual distribution of precipitation is typical to the Mediterranean warm/cool summer climates (Cbs) [36], with a concentration of precipitation in the cold months (between October and March, 72% of annual precipitation). The highest values of average annual precipitation are registered in the zones of higher altitudes (1215.6 mm in Moimenta and 1262.8 mm in Montesinho) and in the western part (1075.1 mm in Vinhais). There is a marked reduction in precipitation towards the east (806 mm in Deilão) resulting, in part, from the Foehn effect, which occurs when air masses cross steep reliefs and progressively dehydrate [32].

Regarding wind speed, the highest monthly average values occur from February to May which coincides with spring. The lowest occur in winter (end of December to February), representing the most frequent stable situations at this time of year. The direction is predominantly from the west throughout the year [32].

Fig. 2 shows the climate diagram for the city of Bragança, using data from meteorological stations between 1960 and 1990 [37]. It can be observed that, between the T_{air} and precipitation, there is an asymmetric distribution, resulting in a deficit of water in the soil in summer, which affects the vegetation that is more sensitive to summer dryness [37].

2.2. Environmental data

We compiled and processed LST data and additional environmental data from several MODIS products for the period 2003–2021, which is the longest continuous time series (Table 1), using Google Earth Engine [38] and QGIS software 3.22 Białowieża [39]. GEE is a cloud-based computational platform [40] that includes the entire Landsat, MODIS, and Sentinel-2 datasets, as well as climatic and

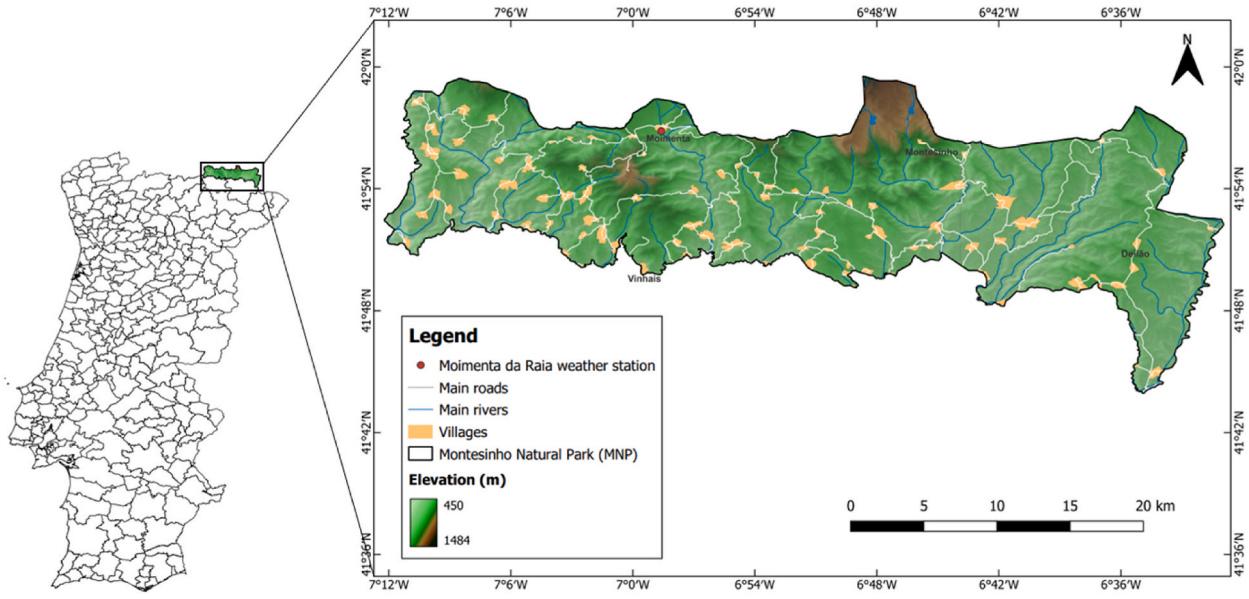

Fig. 1. Overview of the study area - Montesinho Natural Park (MNP) in Bragança (Portugal). Elevation of MNP obtained through the digital model terrain from the Portuguese Directorate General of the Territory [33].

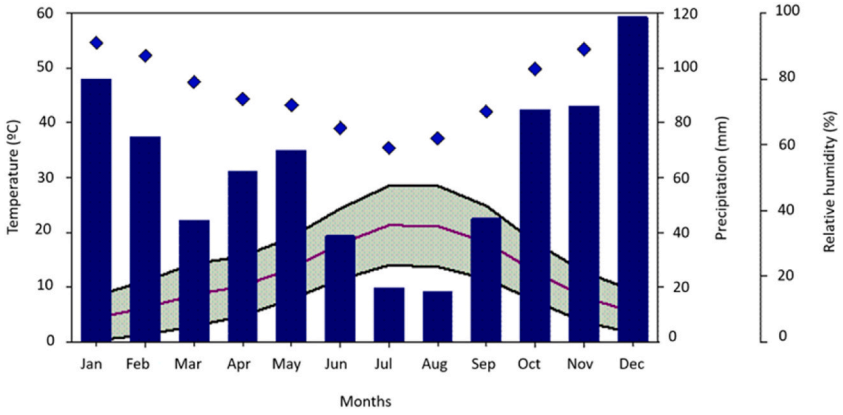

Fig. 2. Monthly variation of the average values of maximum and minimum temperatures, relative humidity and annual distribution of precipitation for Bragança (Portugal) between 1960 and 1990. The monthly precipitation is represented by the columns and the average monthly maximum and minimum temperature values are represented by the band (adapted from Ref. [37]).

elevation data. GEE images are automatically pre-processed (cloud and topographic correction) [41]. We computed and resampled all variables at 1 km grid cells, the minimum spatial resolution common to all products.

We obtained the LST in GEE from the daily data recorded by the Aqua and Terra MODIS sensors, considering the best quality option available ("LST produced, good quality, not necessary to examine more detailed QA"). Considering the capture times of the two sensors in MNP, we compiled the LST data from 11am, 1pm, 10pm and 2am, to measure the temperature variability throughout the day and

Table 1
Comprehensive summary of the environmental variables considered in this study, indicating product name, spatial resolution, rationale, and source.

Product name	Acronym	Product	Pixel size	Rationale	Source
Air Temperature	T_{air}	Air Temperature	Point where the weather station is located	Measures the air temperature values.	National Water Resources Information System
Albedo NIR-White	ALB-NIRW	MCD43B3	500 m	Measures the diffuse reflectivity or reflectance power of a surface.	Google Earth Engine (GEE)
Albedo NIR-Black	ALB-NIRB				
Albedo VIS-White	ALB-VISW				
Albedo VIS-Black	ALB-VISB				
Enhanced Vegetation Index	EVI	MOD13Q1.061	250 m	Vegetation cover quality, productivity, and status.	
Evapotranspiration	ET	MOD16A2.006	500 m	Water balance between the vegetation cover and hydrological cycle.	
Fraction of Absorbed Photosynthetically Active Radiation	FPAR	MCD15A3H.061		Fraction of photosynthetically active radiation (400–700 nm) absorbed by green vegetation.	
Gross Primary Productivity	GPP	MOD17A2H.006		Terrestrial energy, carbon, water cycle processes, and biogeochemistry of vegetation.	
Land Surface Temperature (Terra)	LST_11am LST_10pm	MOD11A2.061	1 km	Energy balance on the earth's surface.	
Land Surface Temperature (Aqua)	LST_1pm LST_2am				
Leaf Area Index	LAI	MCD15A3H.061	500 m	Determines the interface size for energy (including radiation) and mass exchange between the canopy and the atmosphere.	
Normalized Difference Vegetation Index	NDVI	MOD13Q1.061	250 m	Vegetation cover quality, productivity, and status.	
Surface reflectance (620–670 nm)	SR-Band1	MOD09Q1.061		Changes detection and monitoring on the Earth's surface.	
Surface reflectance (841–876 nm)	SR-Band2				
Multi-Scale Topographic Position Index	mTPI	CSP/ERGo/1_0/Global/SRTM_mTPI	270 m	Distinction between ridges and valleys.	
Land Use and Land Cover	LULC	Land use and occupation letters (2007, 2010, 2015, and 2018)	25 m	Land use and cover properties.	Portuguese Directorate General of the Territory (DGT)

not only during the solar period [42]. The night temperature represents the period when the emitted electromagnetic energy accumulates in areas with low albedos and there are no representative influences from clouds and shadows, compared to the daytime period [21]. We divided the data into summer (June, July, and August) and winter (December, January, and February) months to identify whether seasonality influenced the results. These seasons represent the highest and lowest angle of solar electromagnetic energy incidence, respectively [43–45].

We compiled the LULC data from the Portuguese Directorate General of the Territory [33] for the years 2007, 2010, 2015 and 2018, with a spatial resolution of 25 m. We merged the LULC classes from level 1 (Table 2), using QGIS software, to analyse the statistical differences between LULC and LST. To simplify further analyses, we aggregated similar LULC classes and calculated the percentage of each land use category (at 25 m) within each 1 km pixel. In the end, we obtained nine LULC classes (Table 2).

We computed the Multi-Scale Topographic Position Index (mTPI) [46] to analyse the influence of topography on thermal behaviour. The mTPI compares the elevation of each pixel in a Digital Elevation Model (DEM - SRTM Digital Elevation 30 m), with the average altitude on its surroundings distinguishing between ridges and valleys.

2.3. LST and T_{air} relationship

We tested the normality of LST with the Shapiro test and correlated LST and T_{air} with the Spearman test at the geographical point corresponding to the location of the only permanent meteorological station existent in the territory of the MNP, located in Moimenta da Raia (41° 56′ 50.726″ N and 6° 58′ 37.182″ W).

To this end, for each reference hour of the passage of the satellite (11am, 1pm, 10pm and 2am) we obtained the corresponding real times of LST recording of each day within the period under analysis and then we acquired the corresponding T_{air} for those times with a margin of up to ±0h30 in the National Water Resources Information System [47].

For the purpose of standardization, the correlation results were separated into five scales: i) values between 0.00 to ±0.19: null correlation; ii) between ±0.20 to ±0.29: weak correlation; iii) between ±0.30 to ±0.39: moderate correlation; iv) between ±0.40 to ±0.69: strong correlation; and ≥ of ±0.70: very strong correlation [48].

2.4. Statistical analyses

We analysed whether there were differences in LST between LULC classes with the non-parametric Mann-Whitney *U* test (Table 2). We computed the annual average LST for each sensor pass (11am, 1pm, 10pm and 2am), for the summer and winter of 2007, 2010, 2015 and 2018 (which coincide with the years in which LULC data were available), and the percentage of each cell of the LULC grid. We analysed the trends in LST (neutral, increasing, or decreasing) for summer and winter over time, with the Mann-Kendall test using the annual averages of the four LST (11am, 1pm, 10pm, and 2am). Then, we mapped the Mann-Kendall trend tests considering only the significant pixels ($\alpha = 0.05$).

We identified hot and cold LST clusters with Local Indicators of Spatial Association (LISA) analysis, which measures the degree of spatial association between a variable and its geographic distribution in a study area through Local Moran's I with 999 permutations [49]. This method was chosen because it is useful and widely used in identifying spatial autocorrelation patterns and favours the visualization of such clusters from georeferenced data [49–51]. We produced maps for four cluster types (High-High, Low-Low, High-Low and Low-High) for the summer and winter of each year from 2003 to 2021, and for each satellite pass time (11am, 1pm, 10pm and 2am). We analysed the persistence of each cluster type by joining in a single map all the 19-years LISA maps.

We verified whether there were zones with different thermal behaviours over time by analysing the hourly variation in LST during the day and night, based on the different times of passage of the Terra and Aqua sensors. For this purpose, we calculated the variation coefficients using the exact time of passage of the sensors each day, for each cell of the 1 km grid, applying Equations (1) and (2). Note that, the data from LST_2am and Time_2am refer to data from the day after LST_10pm and Time_10pm.

Table 2
Land use and occupation classes from letters (2007, 2010, 2015, and 2018) data provided by the Portuguese Directorate General of Territory [33], used in this study. The table includes the code, name, and description of the classes, which were used to determine the land use and land cover within Montesinho Natural Park.

Class Code	Class	Class description
1	Urban areas	Artificialized Territories
2	Agriculture	Agriculture
3	Pastures	Pastures
4	Agroforestry	Agroforestry areas (SAF) and Chestnut trees
5	Coniferous Forest	Coniferous and Pinus pinaster forest
6	Broadleaf forest	Forest of cork oak, holm oak and other oaks
7	Shrubland	Shrubland
8	Sparse vegetation	Bare rock and sparse vegetation
9	Surface water bodies	Water bodies

$$DayCoefficient = \frac{LST_{1pm} - LST_{11am}}{Time_{1pm} - Time_{11am}} \quad (1)$$

$$NightCoefficient = \frac{LST_{10pm} - LST_{2am}}{24 - Time_{10pm} - Time_{2am}} \quad (2)$$

We considered that a surface temperature inversion occurs when the coefficient of variation is negative, i.e., when the temperature at 1pm is lower than at 11am and when the temperature at 10pm is higher than at 2am of the next day (same night). Finally, we quantified the percentage of surface temperature inversion over the period under analysis.

We analysed the influence of topography on thermal behaviour with a mTPI, resampled from the original scale of 270 m to 1 km by extracting the average values of each grid cell and resulting in mTPI index between −46 and 55 in MNP. Values less than −20 corresponded to valleys and greater than 20 to ridges (values that maximized the valley and ridge areas, without compromising their correct identification). Finally, for the 113 valley points and 101 ridge points obtained with the referred thresholds, we analysed the LST trends with the Mann-Kendall test.

We correlated LST (summer and winter, between 2003 and 2021, and capture time of each sensor: 11am, 1pm, 10pm, and 2am) with various biophysical indices: Albedo Near Infrared - Black (ALB-NIRB), Albedo Near Infrared - White (ALB-NIRW), Albedo Visible - Black (ALB-VISB), Albedo Visible - White (ALB-VISW), Evapotranspiration (ET), Enhanced Vegetation Index (EVI), Fraction of Absorbed Photosynthetically Active Radiation (FPAR), Gross Primary Productivity (GPP), Leaf Area Index (LAI), Normalized Difference Vegetation Index (NDVI), Surface reflectance (620–670 nm) (SR-Band1), and Surface reflectance (841–876 nm) (SR-Band2), to assess whether these indices affected the thermal behaviour [52,53]. All statistical analyses were performed in R version 4.1.0 and GEE.

2.5. Comparison of MODIS results with landsat

We compared the LST values obtained from MODIS images with Landsat LST using two approaches, namely: (i) Landsat 5 from 2003 to 2012 and Landsat 8 from 2013 to 2021, using the "USGS Landsat 5 Level 2, Collection 2, Tier 1" [54] and "USGS Landsat 8 Level 2, Collection 2, Tier 1" [55] collections, respectively. In this case, we adopted approach (ii) Landsat 7 from 2003 to 2021, using the "USGS Landsat 7 Level 2, Collection 2, Tier 1″ collection [56]. Despite covering the entire analysed period (2003–2021), we did not consider the single use of Landsat 7 due to the failure of Scan Line Corrector (SLC) from May 2003 [57], and kept both analyses to evaluate if we could get complementary information.

The acquisition of Landsat images in the study area occurs between 10am and 11am, every 16 days, which allowed us to compare the results only with the MODIS LSTs of 11am, on coincident dates. We applied a cloud mask (using bits 3 and 4 of the QA_PIXEL band to mask the pixels with clouds and cloud shadows) to select the Landsat images. We calculated the LST by applying the sensor inherent scale factors of the thermal band (band "ST_B6" for Landsat 5 and 7 and "ST_B10" for Landsat 8) and by converting the obtained result from Kelvin to Celsius.

For the three Landsat sensors, we calculated the averages of temperature for the entire MNP territory and then, for some time series, calculated the Spearman correlation between MODIS and Landsat 7 and MODIS and Landsat 5 & 8, using exclusively dates where data existed in both sources, separated into: i) all dates (summer + winter) and ii) analysis of the influence of seasonality on the results, separating the data obtained in the aforementioned seasons.

The Mann-Kendall trend test maps analysis was conditioned to the amount of data eligible for its calculation and, due to the time of passage being only in the daytime period, the inversion and trends analysis of surface temperature in the night period could not be applied to Landsat data.

3. Results

3.1. LST and T_{air} relationship

The correlations between LST and T_{air} were very strong and remained consistently higher than 0.7 across all four sensor passage times and both summer and winter seasons (Table 3). Specifically, in the summer season, there was a strong correlation between LST at 10pm and T_{air} ($\rho = 0.935$) and LST at 2am and T_{air} ($\rho = 0.919$). On average, the LST is higher than T_{air} during the day and lower during the night and the differences between those magnitudes during the day are significantly higher in the summer months than in the winter months.

Table 3
Spearman's correlations (ρ) between Air Temperature (T_{air}) and Land Surface Temperature (LST), at each sensor passage time, by seasonality (winter and summer), in Montesinho Natural Park (MNP).

	LST_11am		LST_1pm		LST_10pm		LST_2am	
Season	Nº. of data	ρ	Nº. of data	ρ	Nº. of data	ρ	Nº. of data	ρ
Summer	458	0.731	402	0.709	403	0.935	425	0.919
Winter	178	0.812	185	0.772	167	0.903	179	0.904

3.2. Did temperature increase in the MNP over time?

In general, thermal behaviour was more heterogeneous during winter than summer (Fig. 3). The Mann-Kendall test detected positive trends of LST over time during winter (namely at 10pm and 2am) (Fig. 4). The average Sen's slope values for LST at 11am, LST at 1pm, LST at 10pm, and LST at 2am were 0.092, 0.113, 0.111, and 0.119, respectively. For the summer data, no significant results were obtained. Warm and cold areas of LST were spatially stable in both seasons over time (Fig. 5): some High-High and Low-Low clusters remain in the same place for the whole period (19 years).

In summer, during the daytime the warmest zones were concentrated in the eastern part of the MNP and the coldest ones in the western part, but this pattern was the opposite during winter's night-time period (Fig. 5). During summer nights, the coldest zones corresponded to the highest altitudes (Fig. 5). During the daytime in winter, the clusters were more dispersed throughout the territory, although they also maintain some persistence in location. There were no significant HL and LH clusters.

Considering the satellite passages times, the LST varied more in the day period than at night, and there were more surface temperature inversions in the daytime period of summer and in the night period of winter (Table 4; Figs. 6 and 7). In summer, there was a high percentage of surface temperature inversions dispersed throughout the territory, with some parts of the territory having the LST at 11am higher than the LST at 1pm almost half of the days (Figs. 6 and 7). In this period, there was a location where the average coefficient (Equation (1)) was negative. In winter, temperature variation was low, but there were some parts of the territory with a high percentage of inversions and there were also some parts of the territory that showed a negative coefficient (Equation (2)) between 10pm and 2am. In the daytime periods in winter and night-time in summer, no zones had an average negative coefficient, and the percentage of inversions was lower, with several zones in the territory without inversions.

3.3. What environmental factors influence the LST?

There were no significant differences between LST and LULC classes (Table 5). The mTPI analyses identified 113 pixels as valleys and 101 as ridges out of a total of 857 pixels. For all times of day LST trends were lower in the valleys and higher on the ridges (except for daylight hours in summer). In the case of daytime summer periods, the pattern was the opposite (Table 6).

3.4. Is temperature rise affected by vegetation?

The indexes ET, EVI, FPAR, GPP, LAI and NDVI were highly and negatively correlated with LST in summer at 11am and 1pm (Appendix 1, Table A and Table B). In winter, the indices did not show strong correlations with LST. Except for SR-Band2, the other indices showed strong correlations in at least one of the analysed years (Appendix 1, Table C). Indices presenting correlations in more years were ALB-NIRB, ALB-NIRW, ALB-VISB and ALB-VISW, GPP and NDVI presented the highest correlations, but not all were negative (opposing the pattern observed in the summer).

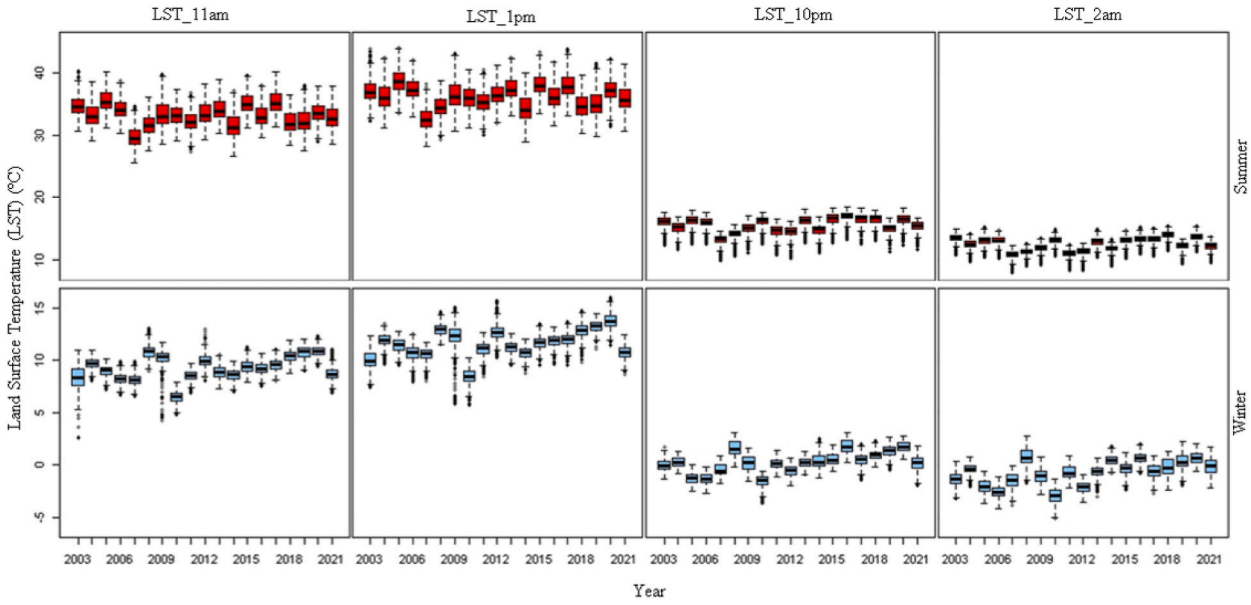

Fig. 3. Boxplots of Land Surface Temperature (LST) (°C) throughout the years (2003–2021) for the different sensor passage time (11am, 1pm, 10pm and 2am) in Montesinho Natural Park (MNP). Boxplots in blue colour refer to winter season and red colour boxplots to summer season.

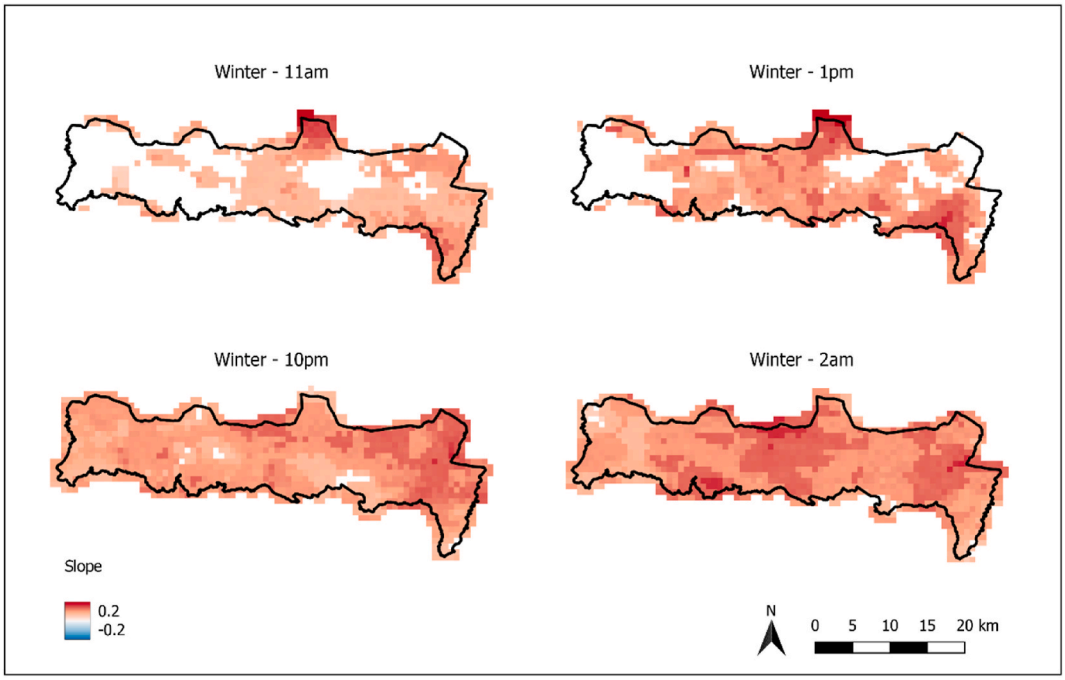

Fig. 4. Mann-Kendall trend test maps for winter season according to each sensor passage time (11am, 1pm, 10pm and 2am) in Montesinho Natural Park (MNP) – with the significant Sen's slope values (−0.2 to 0.2 unitless).

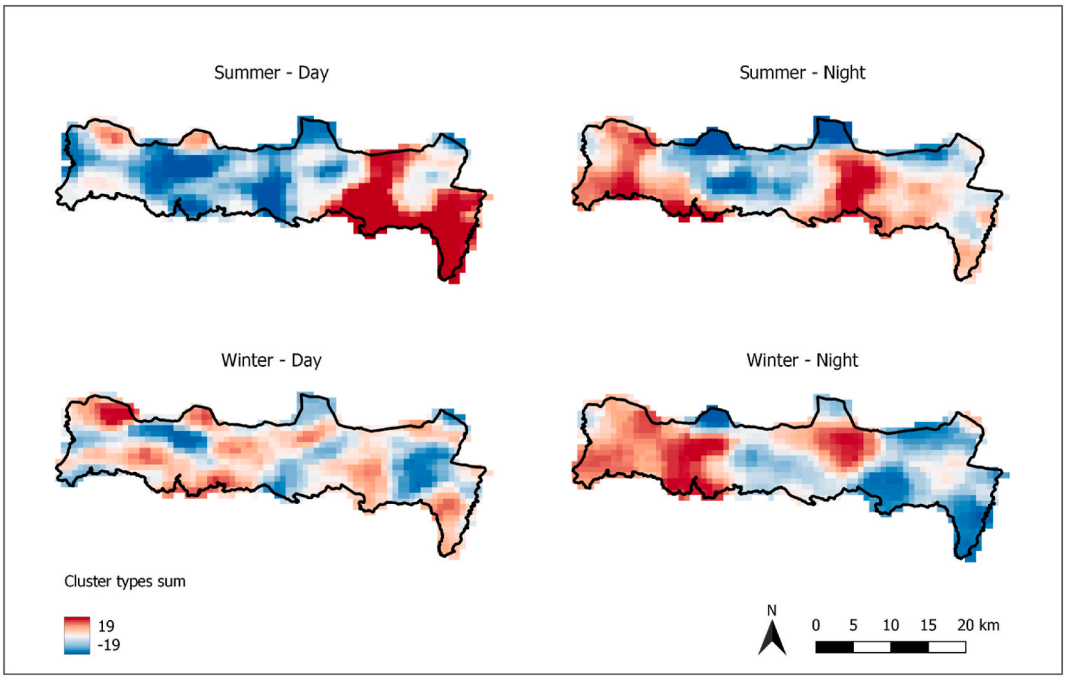

Fig. 5. Cumulative map depicting high-high clusters (0–19 in red) and low-low clusters (-19 - 0 in blue). The map represents time pairs of 11 a.m. and 1 p.m. for daytime and 10 p.m. and 2 a.m. for nighttime in Montesinho Natural Park (MNP).

Table 4
Variation coefficients of average hourly land surface temperature and surface temperature inversion counts per season (summer and winter) and time period (Day - between 11am and 1pm; Night - between 10pm and 2am the following day) in Montesinho Natural Park (MNP) from 2003 to 2021.

MNP 2003–2021		Variation coefficient ($^{o}Ch^{-1}$)	Surface temperature inversion (percentage)
Summer	Day	1.50	20.2%
	Night	0.70	1.9%
Winter	Day	1.44	2.0%
	Night	0.28	9.3%

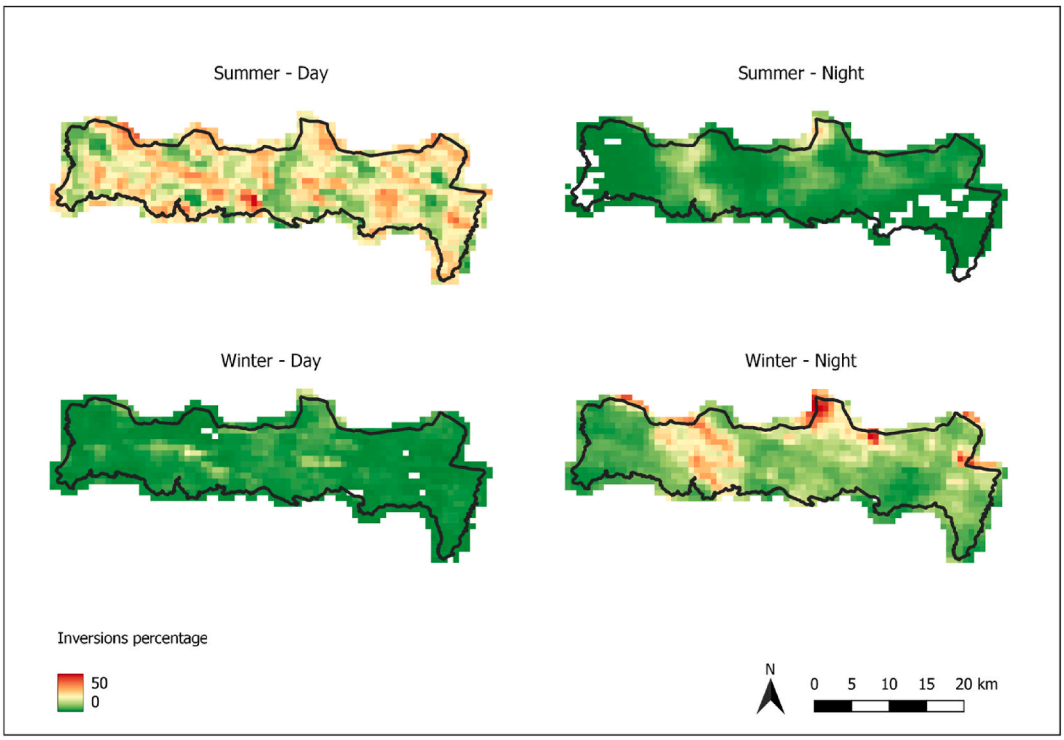

Fig. 6. Surface temperature inversions calculated from Land Surface Temperature (LST) in Montesinho Natural Park (MNP) by season (summer and winter). Values come in percentages (%). The map presents time pairs of 11 a.m. and 1 p.m. for daytime and 10 p.m. and 2 a.m. for nighttime in MNP. The presence of white pixels within some clusters (Winter - Day and Summer – Night) indicates that there is no available data for those specific pixels due to quality treatment.

3.5. Are the MODIS results comparable to landsat?

Considering that the revisit interval of Landsat to the study area is longer than that of MODIS and that we used only valid and coincident images on both satellites for comparison, we had temporal gaps in the eligible images, mainly during winter, although with occasional data shortages during summer (presented in Annex 2, Table A).

The correlations between MODIS and Landsat LST considering both summer and winter images were strong and with close results, namely: $\rho = 0.980$ between MODIS and Landsat 7 data (considering 88 dates) and $\rho = 0.943$ for MODIS and Landsat 5 & 8 data (with 106 dates).

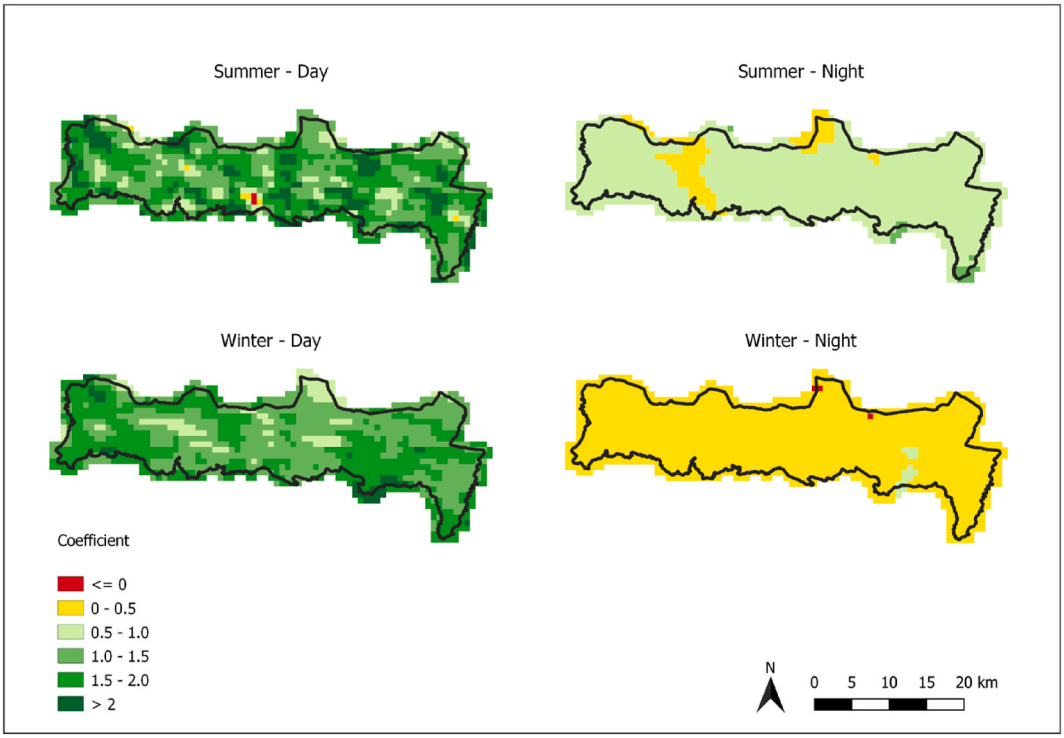

Fig. 7. Hourly variation coefficients of land surface temperature in Montesinho Natural Park (MNP) by season (summer and winter). The map presents time pairs of 11 a.m. and 1 p.m. for daytime and 10 p.m. and 2 a.m. for nighttime in MNP.

Table 5
Significant differences between Land Surface Temperature (LST) and Land Use and Land Cover (LULC) classes, obtained from the land use and occupation letters (2007, 2010, 2015, and 2018), provided by the Portuguese Directorate General of Territory [33], measured with the Mann-Whitney *U* test. The analysis was conducted per season (summer and winter) and at each sensor passage time (11 a.m. and 1 p.m.) in Montesinho Natural Park (MNP).

Year	Season	LST	Class	W	p-value
2007	Summer	11 a.m.	Shrubland	655191	0.9863
2010	Summer	1 p.m.	Agriculture	646091	0.5535
2015	Summer	1 p.m.	Agriculture	644352	0.4824
2015	Winter	1 p.m.	Pastures	678312	0.1439
2018	Summer	1 p.m.	Agriculture	638730	0.2901

Considering seasonality, correlations remain strong. In summer, $\rho = 0.929$ for MODIS and Landsat 7 data (55 dates) and $\rho = 0.840$ for MODIS and Landsat 5 & 8 data (71 dates). In winter, $\rho = 0.947$ between MODIS and Landsat 7 data (33 dates) and $\rho = 0.750$ for MODIS and Landsat 5 & 8 data (35 dates).

4. Discussion

Our study indicated significant changes in temperature over time in MNP. Over the 19 years, there is a trend for an average annual increase is the LST on winter nights and remained homogeneous during summer (day and night) and winter daytime, as observed in a similar study [58]. Warmer areas in summer corresponded to cold areas in winter. However, some areas of warm and cold temperatures remained stable over time. There were milder temperatures in the west, which may be associated with a higher incidence of rain and humidity [32].

Table 6
Influence of topography in Land Surface Temperature (LST) trends over time (2003–2021) in Montesinho Natural Park (MNP). Average trends of LST over time (Sen's Slope) in summer and winter for valleys and ridges defined by the Multi-Scale Topographic Position Index (mTPI).

Season	LST	MNP (Valleys and Ridges)	Valleys	Ridges	% dif Valleys -MNP	% dif Ridges -MNP
Summer	11am	−0.027	−0.034	−0.023	20.50%	−19.30%
	1pm	−0.025	−0.033	−0.019	24.40%	−31.40%
	10pm	0.043	0.041	0.044	−4.60%	1.50%
	2am	0.045	0.044	0.048	−2.60%	5.50%
Winter	11am	0.077	0.064	0.077	−18.90%	0.90%
	1pm	0.100	0.083	0.102	−20.20%	2.40%
	10pm	0.109	0.105	0.113	−4.80%	2.70%
	2am	0.117	0.111	0.121	−5.60%	2.70%

In this study, topography had an influence over LST: in valley areas the trends are smoothed, and, in the peaks, they are increased, relative to the general trends of the territory, except for the summer daylight hours, which presented an opposite pattern. Altitude affects LST, generating a gradient that determines that as one moves higher above sea level, there is a tendency for surface temperature to decrease [11,59–61]. However, this relationship is influenced by other factors such as LULC [11,59], elevation range [62], and meteorological conditions [60]. In specific atmospheric conditions, a temperature inversion layer can appear being characterized by the presence of a layer of warm air positioned above cooler air near the surface. In these circumstances, LST within the inversion layer might exhibit an ascent with altitude, contrary to the typical decline in temperature observed at higher elevations [63,64]. This phenomenon can be influenced by the stability of meteorological conditions and specific processes associated with the local orography [65,66]. One process in mountain regions is the formation of katabatic winds (i.e. a drainage wind that carries high-density air from a higher elevation down a slope under the force of gravity), which may determine the formation of a thermal inversion mostly during nocturnal conditions [67].

LST was highly and negatively correlated with the biophysical indices ET, EVI, FPAR, GPP, LAI and NDVI, especially at 11am and 1pm. Vegetation adapts to seasonality: during summer temperature peaks, vegetation enters an estivation state, reducing its metabolic activities for protection from heat and drought, as confirmed by our results, in the aforementioned biophysical indices (i.e., pixels with higher temperatures presented lower values of biophysical indices) [68–70]. In winter, they usually behave similarly to protect themselves from the cold, namely dormancy [70], but in our data, we did not have significant correlation results that ratify the literature. Most areas exhibited a consistent thermal trend throughout each season. The use of day-time and night-time data obtained at different satellite pass times corroborated the heat exchange processes and variations in solar radiation [13,71,72]. Additionally, the inclusion of seasonal analyses also allowed for the understanding of different thermal patterns between seasons [73]. These analyses were possible thanks to the effectiveness of RS in mapping temperature trends: although temperature data can be interpolated from meteorological stations [74], RS data provides temperature data over large areas and over time [75]. Further, analyses can be processed with GEE more quickly and over larger datasets [40].

LST and T_{air} had similar trend patterns over time and strong correlations at the times of passage. Previous studies have obtained similar results to ours, where LST is higher than T_{air} in the morning and lower at night [76,77] and both variables are less correlated during the day than at night [78]. However, as we only have one site for T_{air} and the low spatial resolution of the MODIS sensor (1 km), any conclusion about the representativeness of the results for the whole territory should be considered with caution. Therefore, this site of T_{air} cannot be considered an added value for this work. It is worth noting that the physical variable measured at LST – via radiation – is not the same as at T_{air}, but both refer to surface warming that subsequently affects T_{air} in the lower atmosphere [79], i.e. it is interesting to compare the trends of both variables over time [24,76,80].

Regarding the comparison of LST MODIS and Landsat, the results indicated a strong correlation between the surface thermal behaviour of the areas, both considering all coincident dates (summer + winter) and seasonality. In summer, the number of available images was higher, which may be associated with the presence of clouds and rainfall in the winter period. This result is interesting both to present a similarity in the results obtained in RS from different satellites and to present the comparability between the data acquired by MODIS and Landsat, despite the difference between spatial and temporal resolutions. The revisit time of Landsat, which is more spaced compared to MODIS, compromised the application of temporal and trend analysis due to the number of available images. The revisit time of Landsat only at one time period (11am) makes it impossible to carry out studies that aim to evaluate the thermal behaviour of the surface considering night periods and not allowed the identification surface temperature inversions [21,24,25]. As such, MODIS is a more appropriate data source for these case studies, despite its low spatial resolution in comparison to Landsat or other satellite series with moderate to high spatial resolution.

Future studies should include *in situ* validation data obtained from portable weather stations, data loggers, thermal data from unmanned aerial vehicles (UAV), and handheld thermal cameras, to complement the spatial resolution obtained in MODIS and, consequently, the detail of the analyses [81].

However, the adoption of these suggestions depends on a feasibility analysis and adaptations, considering the specificities of the MNP, especially in relation to its extension: which can make it difficult to collect continuous data. UAV flights, for example, can be used in small areas of heterogeneous coverage for comparison of surface thermal behaviour relative to satellite data or that provide interesting details for the studies. The same applies to the use of portable thermal cameras and portable weather stations. In all approaches, it is necessary to consider the different influences and scale of data for each methodology for the comparison to be appropriate.

5. Conclusions

Climate change contributes to an increase in the intensity and frequency of extreme events, which can contribute to environmental disasters, changes in the hydrological cycle, and impacts on natural biomes and human communities. Mountain systems, as ecologically sensitive areas, are specially affected by these changes, increasing the melting of glaciers, landslides, changes in habitats, and shifts in species ecological niches.

The use of spatial methods that integrate various sources of information, computing tools and statistical analyses proved to be effective for mapping the thermal behaviour.

Indeed, our methodology can be applied to other mountainous areas of similar characteristics, to complement decision-making processes. Research studies aiming to understand the thermal behaviour and trends of mountainous areas are fundamental to identifying patterns and taking remedial and mitigating measures to ensure the conservation and preservation of local biodiversity and ecological services.

Author contribution statement

Ana Cláudia Teodoro; Nuno Garcia; João C. Campos; Salvador Arenas-Castro; Artur Gonçalves; Neftalí Sillero: Conceived and designed the experiments; Analysed and interpreted the data; Contributed reagents, materials, analysis tools or data; Wrote the paper. Cátia Rodrigues de Almeida; João Alírio: Conceived and designed the experiments; Performed the experiments; Analysed and interpreted the data; Contributed reagents, materials, analysis tools or data; Wrote the paper.

Data availability statement

Data will be made available on request.

Declaration of competing interest

The authors declare that they have no known competing financial interests or personal relationships that could have appeared to influence the work reported in this paper.

Acknowledgements

This research was supported by Portuguese national funds through FCT – Foundation for Science and Technology I.P., Portugal under the project MontObEO - Montesinho biodiversity observatory: an Earth Observation tool for biodiversity conservation (FCT: MTS/BRB/0091/2020). This publication is also part of the TED2021-131722B-I00 project, funded by MCIN/AEI/10.13039/501100011033 and by the European Union "NextGenerationEU"/PRTR. Recovery, Transformation and Resilience Plan - Funded by the European Union – NextGenerationEU. CRdA was financially supported by Portuguese national funds through FCT - Foundation for Science and Technology I.P. (Grant: PRT/BD/153518/2021). JCC is supported by a contract under the scope of the MontObEO Project (MTS/BRB/0091/2020), funded by FCT. SAC is supported by the María Zambrano program funded by the Spanish Ministry of Universities and the University of Cordoba (Spain) (Next Generation EU fund). NS is supported by a CEEC2017 contract (CEECIND/02213/2017) from FCT. NG is supported by a research grant from MontObEO project (MTS/BRB/0091/2020). CIMO is supported through national funds (UIDB/00690/2020 and UIDP/00690/2020) and SusTEC (LA/P/0007/2020).

Appendix 1

Table A
Spearman's correlations (ρ) between Land Surface Temperature at 11 a.m. (LST_11am) during the summer period and the environmental variables considered in this study. (in red: null correlation; in orange: weak correlation; in blue: moderate correlation; in green: strong correlation; in black: very strong correlation).

Biophysical Index	2003	2004	2005	2006	2007	2008	2009	2010	2011	2012	2013	2014	2015	2016	2017	2018	2019	2020	2021
ALB-NIRB	−0.14	−0.18	−0.03	−0.14	−0.22	−0.1	−0.26	−0.25	0.06	−0.13	−0.13	−0.15	0	−0.15	0.03	−0.31	−0.12	0.03	−0.1
ALB-NIRW	−0.17	−0.2	−0.08	−0.17	−0.24	−0.12	−0.32	−0.28	0.04	−0.17	−0.14	−0.18	−0.02	−0.17	0	−0.34	−0.16	−0.02	−0.14
ALB-VISB	0.47	0.46	0.53	0.46	0.47	0.5	0.5	0.44	0.58	0.49	0.45	0.49	0.52	0.44	0.53	0.38	0.5	0.55	0.51
ALB-VISW	0.45	0.46	0.52	0.46	0.46	0.49	0.49	0.43	0.57	0.48	0.45	0.49	0.52	0.45	0.54	0.39	0.48	0.56	0.52
ET	−0.75	−0.77	−0.75	−0.72	−0.73	−0.7	−0.81	−0.77	−0.64	−0.73	−0.75	−0.74	−0.67	−0.74	−0.69	−0.77	−0.7	−0.62	−0.71
EVI	−0.72	−0.74	−0.72	−0.71	−0.7	−0.66	−0.79	−0.77	−0.58	−0.7	−0.7	−0.69	−0.61	−0.68	−0.65	−0.76	−0.64	−0.56	−0.62
FPAR	−0.79	−0.79	−0.81	−0.77	−0.75	−0.72	−0.84	−0.81	−0.69	−0.78	−0.78	−0.76	−0.71	−0.77	−0.72	−0.8	−0.72	−0.67	−0.73
GPP	−0.75	−0.78	−0.77	−0.73	−0.69	−0.7	−0.82	−0.77	−0.65	−0.72	−0.74	−0.74	−0.69	−0.72	−0.71	−0.77	−0.7	−0.61	−0.7
LAI	−0.73	−0.76	−0.77	−0.7	−0.71	−0.69	−0.82	−0.76	−0.67	−0.72	−0.74	−0.73	−0.69	−0.73	−0.7	−0.74	−0.7	−0.64	−0.7
NDVI	−0.75	−0.77	−0.8	−0.75	−0.74	−0.75	−0.82	−0.79	−0.71	−0.77	−0.78	−0.75	−0.72	−0.77	−0.73	−0.79	−0.72	−0.71	−0.76
SR-Band1	0.43	0.44	0.46	0.42	0.51	0.4	0.45	0.36	0.5	0.39	0.4	0.44	0.48	0.42	0.47	0.32	0.47	0.48	0.48
SR-Band2	−0.29	−0.32	−0.18	−0.26	−0.34	−0.26	−0.41	−0.4	−0.1	−0.32	−0.27	−0.28	−0.14	−0.26	−0.11	−0.45	−0.25	−0.12	−0.2

Table B
Spearman's correlations (ρ) between Land Surface Temperature at 1 p.m. (LST_1pm) during the summer period and the environmental variables considered in this study. (in red: null correlation; in orange: weak correlation; in blue: moderate correlation; in green: strong correlation; in black: very strong correlation).

Biophysical Index	2003	2004	2005	2006	2007	2008	2009	2010	2011	2012	2013	2014	2015	2016	2017	2018	2019	2020	2021
ALB-NIRB	−0.04	−0.14	0.05	−0.01	−0.2	−0.08	−0.17	−0.21	0.08	−0.02	−0.01	−0.11	0.07	−0.1	0.06	−0.23	−0.06	0.13	−0.06
ALB-NIRW	−0.07	−0.16	0.01	−0.04	−0.22	−0.1	−0.23	−0.24	0.06	−0.06	−0.03	−0.14	0.05	−0.12	0.03	−0.27	−0.11	0.08	−0.1
ALB-VISB	0.55	0.49	0.58	0.57	0.5	0.53	0.58	0.48	0.6	0.58	0.53	0.54	0.56	0.49	0.55	0.44	0.54	0.61	0.55
ALB-VISW	0.52	0.47	0.55	0.56	0.47	0.5	0.55	0.45	0.58	0.56	0.51	0.53	0.54	0.47	0.54	0.44	0.51	0.6	0.54
ET	−0.74	−0.76	−0.72	−0.71	−0.75	−0.72	−0.81	−0.79	−0.68	−0.72	−0.72	−0.77	−0.65	−0.76	−0.7	−0.76	−0.7	−0.6	−0.72
EVI	−0.7	−0.73	−0.68	−0.68	−0.71	−0.68	−0.76	−0.77	−0.61	−0.66	−0.64	−0.7	−0.58	−0.69	−0.66	−0.72	−0.63	−0.51	−0.63
FPAR	−0.79	−0.8	−0.79	−0.76	−0.77	−0.75	−0.83	−0.84	−0.74	−0.78	−0.77	−0.79	−0.7	−0.8	−0.75	−0.79	−0.72	−0.65	−0.75
GPP	−0.74	−0.77	−0.74	−0.72	−0.72	−0.72	−0.81	−0.79	−0.7	−0.73	−0.73	−0.77	−0.68	−0.74	−0.72	−0.77	−0.7	−0.6	−0.72
LAI	−0.75	−0.77	−0.77	−0.73	−0.75	−0.72	−0.83	−0.8	−0.73	−0.75	−0.75	−0.77	−0.7	−0.77	−0.74	−0.75	−0.71	−0.64	−0.74
NDVI	−0.78	−0.79	−0.81	−0.79	−0.77	−0.78	−0.85	−0.82	−0.76	−0.8	−0.81	−0.79	−0.75	−0.81	−0.78	−0.81	−0.74	−0.72	−0.79
SR-Band1	0.51	0.47	0.53	0.52	0.55	0.43	0.54	0.41	0.53	0.48	0.49	0.49	0.54	0.48	0.52	0.39	0.51	0.55	0.52
SR-Band2	−0.21	−0.29	−0.1	−0.16	−0.32	−0.27	−0.34	−0.38	−0.1	−0.24	−0.16	−0.26	−0.08	−0.22	−0.1	−0.38	−0.2	−0.03	−0.18

Table C
Spearman's correlations (ρ) between Land Surface Temperature (LST) at each sensor passage time (11am, 1pm, 10pm and 2am) in Montesinho Natural Park (MNP) during the winter period for each year (2003–2021). Only strong results (in green).

LST	Index	2003	2004	2005	2006	2007	2008	2009	2010	2012	2013	2014	2015	2016	2017	2018	2019	2020	2021
LST_11am	ALB-NIRB			0.41	0.41	0.47				0.43	0.56			0.46	0.55			0.41	
LST_1pm							0.4			0.45	0.4	0.46							
LST_2am									0.41										
LST_11am	ALB-NIRW			0.41	0.43	0.48				0.42	0.55			0.45	0.55			0.41	
LST_1pm							0.4			0.51	0.43	0.48							
LST_2am									0.45										
LST_11am	ALB-VISB		0.46	0.49	0.41	0.48				0.55	0.6		0.47	0.43	0.59	0.44	0.44		
LST_1pm										0.54	0.44	0.52	0.42	0.42	0.45				
LST_11am	ALB-VISW		0.46	0.48	0.41	0.47				0.54	0.6		0.47	0.43	0.59	0.43	0.43	0.4	
LST_1pm										0.55	0.46	0.53	0.42	0.41	0.46				
LST_10pm	EVI						0.4												
LST_2am							0.44												
LST_10pm	FPAR															0.47			
LST_2am														0.46					
LST_10pm	GPP		0.5			0.53	0.53							0.47	0.4	0.43			
LST_2am						0.61	0.44							0.43					
LST_10pm	LAI													0.43	0.4	0.49			
LST_2am														0.44					
LST_11am	NDVI		−0.45							−0.47	−0.48				−0.48				−0.4
LST_10pm										0.4					0.4				
LST_1pm			−0.41							−0.45		−0.53		−0.43	−0.48				−0.41
LST_11am	SR-Band1		0.46																0.55
LST_10pm		−0.4					0.42	0.55											
LST_1pm			0.44							0.41		0.41		0.42				0.53	
LST_2am		−0.4					0.45	0.45											
LST_11am	SR-Band2										0.49			0.41	0.4				
LST_10pm							0.43												
LST_1pm										0.42								0.45	
LST_2am							0.49												

Appendix 2

Table A
Number of images processed to generate the Land Surface Temperature (LST) from Landsat 5 and 8, Landsat 7, and MODIS in winter (W) (Dec, Jan and Feb) and summer (S) (Jun, Jul and Aug).

	Landsat 5 and 8								Landsat 7								MODIS							
	Month						By Season		Month						By Season		Month						By Season	
Year	Jan	Feb	Jun	Jul	Aug	Dec	S	W	Jan	Feb	Jun	Jul	Aug	Dec	S	W	Jan	Feb	Jun	Jul	Aug	Dec	S	W
2003				2	1		3	0		1					0	1	31	28	30	31	31	24	92	83
2004	2	1	1	2	2	2	5	5	1		1				1	1	31	29	30	31	31	31	92	91
2005	2		2	1	1		4	2				1	2	1	3	1	31	28	30	31	31	31	92	90
2006		2	1	2	1	1	4	3			2	1	2	1	5	1	31	28	30	31	31	31	92	90
2007	1	2	1	2	1		4	3	1					1	0	2	31	28	30	31	31	31	92	90
2008				1	2		3	0	1			1	1		2	1	31	29	30	31	31	29	92	89
2009	2	1	1	2	2		5	3	1	1		1	1		2	2	31	28	30	31	31	31	92	90
2010	1	1	1	1	1	1	3	3				1	1		2	0	31	28	30	31	31	31	92	90
2011	2		2	1	1		4	2							0	0	31	28	30	31	31	31	92	90
2012							0	0	1	2			1		1	3	31	29	30	31	31	31	92	91
2013			2	2	1	2	5	2			1			1	1	1	31	28	30	31	31	31	92	90
2014	1	1	1	2	2	2	5	4	1	1	2	2	2	2	6	4	31	28	30	31	31	31	92	90
2015	2	1	2	2	2	1	6	4	1	1	2	2	2	1	6	3	31	28	30	31	31	31	92	90
2016	2	1	2	2	2	1	6	4	1	1	2	2	1	2	5	4	31	20	30	31	31	31	92	82
2017	2	1	2	2	2	2	6	5	2	1	1	2	2	2	5	5	31	28	30	31	31	31	92	90
2018	1	2	2	2	2	1	6	4	1	1	2	2	2	1	6	3	31	28	30	31	31	31	92	90
2019	2	2	2	1	2	2	5	6	2	1	2	2	2	1	6	4	31	28	30	31	31	31	92	90
2020	1	2	1	2	2	2	5	5	1	1	2	2	2	2	6	4	31	29	30	31	31	31	92	91
2021	1	1	2	2	2	1	6	3	2	2	2	2	2	1	6	5	31	28	30	31	31	31	92	90
Total	22	18	25	31	29	18	85	58	16	13	19	21	23	16	63	45	589	528	570	589	589	580	1748	1697

References

[1] R.G. Barry, in: Mountain Weather and Climate, Cambridge, 2008.
[2] M.M. Kling, D.D. Ackerly, Global wind patterns and the vulnerability of wind-dispersed species to climate change, Nat. Clim. Change 10 (2020) 868–875, https://doi.org/10.1038/s41558-020-0848-3.
[3] G. Hansen, D. Stone, Assessing the observed impact of anthropogenic climate change, Nat. Clim. Change 6 (2016) 532–537, https://doi.org/10.1038/nclimate2896.
[4] R.P. Allan, M. Barlow, M.P. Byrne, A. Cherchi, H. Douville, H.J. Fowler, T.Y. Gan, A.G. Pendergrass, D. Rosenfeld, A.L.S. Swann, et al., Advances in understanding large-scale responses of the water cycle to climate change, Ann. N. Y. Acad. Sci. 1472 (2020) 49–75, https://doi.org/10.1111/nyas.14337.
[5] G. Luber, M. McGeehin, Climate change and extreme heat events, Am. J. Prev. Med. 35 (2008) 429–435, https://doi.org/10.1016/j.amepre.2008.08.021.
[6] S.R. Loarie, P.B. Duffy, H. Hamilton, G.P. Asner, C.B. Field, D.D. Ackerly, The velocity of climate change, Nature 462 (2009) 1052–1055, https://doi.org/10.1038/nature08649.
[7] N. Sillero, Climate change in action: local elevational shifts on Iberian amphibians and reptiles, Reg. Environ. Change 21 (2021) 101, https://doi.org/10.1007/s10113-021-01831-w.
[8] J. Geletič, M. Lehnert, P. Dobrovolný, Land surface temperature differences within local climate zones, Based on two central European cities, Rem. Sens. 8 (2016) 1–18, https://doi.org/10.3390/rs8100788.
[9] X. Yang, L. Yao, T. Jin, L.L.H. Peng, Z. Jiang, Z. Hu, Y. Ye, Assessing the thermal behavior of different local climate zones in the Nanjing metropolis, China, Build. Environ. 137 (2018) 171–184, https://doi.org/10.1016/j.buildenv.2018.04.009.
[10] C. Fricke, R. Pongrácz, T. Gál, S. Savić, J. Unger, Using local climate zones to compare remotely sensed surface temperatures in temperate cities and hot desert cities, Morav. Geogr. Rep. 28 (2020) 48–60, https://doi.org/10.2478/mgr-2020-0004.
[11] F. Taripanah, A. Ranjbar, Quantitative analysis of spatial distribution of land surface temperature (LST) in relation Ecohydrological, terrain and socio- economic factors based on Landsat data in mountainous area, Adv. Space Res. 68 (2021) 3622–3640, https://doi.org/10.1016/j.asr.2021.07.008.
[12] C. Aguiar, O. Rodrigues, J. Azevedo, T. Domingos, H.M. Pereira, T. Domingos, L. Vicente, V. Proença (Eds.), Bragança - Portugal, 2009.
[13] J.C. Azevedo, V. Cadavez, M. Arrobas, J.M. Pires, Sustentabilidade da montanha portuguesa: realidades, Sustentabilidade da Mont. Port. Real. e Desafios. Bragança, IPB 9–38 (2016).
[14] J. Xu, R.E. Grumbine, A. Shrestha, M. Eriksson, X. Yang, Y. Wang, A. Wilkes, The melting himalayas: cascading effects of climate change on water, biodiversity, and livelihoods, Conserv. Biol. 23 (2009) 520–530, https://doi.org/10.1111/j.1523-1739.2009.01237.x.
[15] B.G. Mark, A. French, M. Baraer, M. Carey, J. Bury, K.R. Young, M.H. Polk, O. Wigmore, P. Lagos, R. Crumley, et al., Glacier loss and hydro-social risks in the Peruvian Andes, Global Planet. Change 159 (2017) 61–76, https://doi.org/10.1016/j.gloplacha.2017.10.003.
[16] M. Beniston, The Risks Associated with Climatic Change in Mountain Regions, 2005, pp. 511–519.
[17] F. Médail, K. Diadema, Glacial refugia influence plant diversity patterns in the Mediterranean Basin, J. Biogeogr. 36 (2009) 1333–1345, https://doi.org/10.1111/j.1365-2699.2008.02051.x.
[18] N. Sillero, J. RibeiroSilva, S. ArenasCastro, Shifts in climatic realised niches of Iberian species, Oikos 2022 (2022), https://doi.org/10.1111/oik.08505.
[19] M.E. Rocca, P.M. Brown, L.H. MacDonald, C.M. Carrico, Climate change impacts on fire regimes and key ecosystem services in Rocky Mountain forests, For. Ecol. Manage. 327 (2014) 290–305, https://doi.org/10.1016/j.foreco.2014.04.005.
[20] M. Neteler, Estimating daily land surface temperatures in mountainous environments by reconstructed MODIS LST data, Rem. Sens. 2 (2010) 333–351, https://doi.org/10.3390/rs1020333.
[21] C.R. de Almeida, A.C. Teodoro, A. Gonçalves, Study of the urban heat island (UHI) using remote sensing data/techniques: a systematic review, Environments 8 (2021) 105, https://doi.org/10.3390/environments8100105.
[22] G.C. Hulley, D. Ghent, F.M. Göttsche, P.C. Guillevic, D.J. Mildrexler, C. Coll, Land Surface Temperature, 2019.
[23] P. Guillevic, F. Göttsche, J. Nickeson, G. Hulley, D. Ghent, Y. Yu, I. Trigo, S. Hook, J.A. Sobrino, J. Remedios, et al., Land surface temperature product validation best practice protocol version 1.1, Best Pract. Satell. L. Prod. Valid. (2018) 60, https://doi.org/10.5067/doc/ceoswgcv/lpv/lst.001.
[24] C.R. de Almeida, L. Furst, A. Gonçalves, A.C. Teodoro, Remote sensing image-based analysis of the urban heat island effect in Bragança, Portugal, Environ. - MDPI (2022) 9, https://doi.org/10.3390/environments9080098.
[25] C.L. Errea, C.R. de Almeida, A. Gonçalves, A.C. Teodoro, Remote sensing analysis of the surface urban heat island effect in vitoria-gasteiz, 1985 to 2021, Rem. Sens. 15 (2023) 3110, https://doi.org/10.3390/rs15123110.
[26] M.L. Imhoff, P. Zhang, R.E. Wolfe, L. Bounoua, Remote sensing of the urban heat island effect across biomes in the continental USA, Remote Sens. Environ. 114 (2010) 504–513, https://doi.org/10.1016/j.rse.2009.10.008.
[27] Eumetsat SEVIRI. https://www.eumetsat.int/seviri, 2022.
[28] S.C. Freitas, I.F. Trigo, J. Macedo, C. Barroso, R. Silva, R. Perdigão, Land surface temperature from multiple geostationary satellites, Int. J. Rem. Sens. 34 (2013) 3051–3068, https://doi.org/10.1080/01431161.2012.716925.
[29] NOAA Geostationary Operational Environmental Satellites (GOES), 2022. https://www.ospo.noaa.gov/Operations/GOES/index.html.
[30] J. Castro, Land use, landscape and sustainability: examples from Montesinho, in: Natural Heritage from East to West, Springer Berlin Heidelberg, Berlin, Heidelberg, 2010, pp. 151–154.
[31] J. Castro, T. de Figueiredo, F. Fonseca, J.P. Castro, S. Nobre, L.C. Pires, Montesinho natural Park: general description and natural values, in: Natural Heritage from East to West, Springer Berlin Heidelberg, Berlin, Heidelberg, 2010, pp. 119–132.
[32] Instituto da Conservação da Natureza e das Florestas (ICNF), Parque Natural de Montesinho, 2022. https://icnf.pt/conservacao/parques/parquenaturaldemontesinho.
[33] Direção-Geral do Território (Dgt), Dados abertos. https://www.dgterritorio.gov.pt/dados-abertos, 2022.
[34] K. McCaffrey, J.M. Wilczak, L. Bianco, E. Grimit, J. Sharp, R. Banta, K. Friedrich, H.J.S. Fernando, R. Krishnamurthy, L.S. Leo, et al., Identification and characterization of persistent cold pool events from temperature and wind profilers in the columbia river basin, J. Appl. Meteorol. Climatol. 58 (2019) 2533–2551, https://doi.org/10.1175/JAMC-D-19-0046.1.
[35] J. Castro, M. Castro, A. Gómez-Sal, Changes on the climatic edge: adaptation of and challenges to pastoralism in Montesinho (northern Portugal), Mt. Res. Dev. (2021) 41, https://doi.org/10.1659/MRD-JOURNAL-D-21-00010.1.
[36] W. Köppen, Versuch einer Klassifikation der Klimate, vorzugsweise nach ihren Beziehungen zur Pflanzenwelt, Geogr. Z. 6 (1900) 657–679.
[37] A. Gonçalves, A.C. Ribeiro, M. Feliciano, F. Maia, Clima Urbano de la Ciudad de Bragança, 2014.
[38] Google Earth engine. https://earthengine.google.com, 2022.
[39] QGIS 3.22, 2022. Białowieża, https://blog.qgis.org/2021/10/30/qgis-3-22-bialowieza-is-released/.
[40] N. Gorelick, M. Hancher, M. Dixon, S. Ilyushchenko, D. Thau, R. Moore, Google Earth engine: planetary-scale geospatial analysis for everyone, Remote Sens. Environ. 202 (2017) 18–27, https://doi.org/10.1016/j.rse.2017.06.031.
[41] K. Hurni, A. Heinimann, L. Google Würsch, Earth Engine Image Pre-processing Tool : Background and Methods, 12, 2017.
[42] S. Peng, S. Piao, P. Ciais, P. Friedlingstein, C. Ottle, F.-M. Bréon, H. Nan, L. Zhou, R.B. Myneni, Surface urban heat island across 419 global big cities, Environ. Sci. Technol. 46 (2012) 696–703, https://doi.org/10.1021/es2030438.
[43] J. Zhou, D. Hu, Q. Weng, Analysis of surface radiation budget during the summer and winter in the metropolitan area of Beijing, China, J. Appl. Remote Sens. 4 (2010), 043513, https://doi.org/10.1117/1.3374329.
[44] M. Santamouris, C. Cartalis, A. Synnefa, Local urban warming, possible impacts and a resilience plan to climate change for the historical center of Athens, Greece, Sustain. Cities Soc. 19 (2015) 281–291, https://doi.org/10.1016/j.scs.2015.02.001.
[45] M. Wang, Z. Zhang, T. Hu, G. Wang, G. He, Z. Zhang, H. Li, Z. Wu, X. Liu, An efficient framework for producing landsat-based land surface temperature data using Google Earth engine, IEEE J. Sel. Top. Appl. Earth Obs. Rem. Sens. 13 (2020) 4689–4701, https://doi.org/10.1109/JSTARS.2020.3014586.

[46] Y. Chen, Y. Wei, Q. Wang, F. Chen, C. Lu, S. Lei, Mapping post-earthquake landslide susceptibility: a U-net like approach, Rem. Sens. 12 (2020) 2767, https://doi.org/10.3390/rs12172767.
[47] SNIRH Sistema Nacional de Informação de Recursos Hídricos, 2022. https://snirh.apambiente.pt/.
[48] C. Dancey, J. Reidy, Statistics without Maths for Psychology, seventh ed., Pearson Education, Harlow, United Kingdom, 2017.
[49] L. Anselin, Local indicators of spatial association-LISA, Geogr. Anal. 27 (1995) 93–115, https://doi.org/10.1111/j.1538-4632.1995.tb00338.x.
[50] L. Anselin, Spatial externalities, spatial multipliers, and spatial econometrics, Int. Reg. Sci. Rev. 26 (2003) 153–166, https://doi.org/10.1177/0160017602250972.
[51] B. Boots, Local measures of spatial association, Ecoscience 9 (2002) 168–176, https://doi.org/10.1080/11956860.2002.11682703.
[52] V. Muradyan, G. Tepanosyan, S. Asmaryan, A. Saghatelyan, F. Dell'Acqua, Relationships between NDVI and climatic factors in mountain ecosystems: a case study of Armenia, Remote Sens. Appl. Soc. Environ. 14 (2019) 158–169, https://doi.org/10.1016/j.rsase.2019.03.004.
[53] A.A. Bindajam, J. Mallick, S. AlQadhi, C.K. Singh, H.T. Hang, Impacts of vegetation and topography on land surface temperature variability over the semi-arid mountain cities of Saudi arabia, Atmosphere 11 (2020) 762, https://doi.org/10.3390/atmos11070762.
[54] Earth engine data catalog search USGS Landsat 5 level 2. https://developers.google.com/earth-engine/datasets/catalog/LANDSAT_LT05_C02_T1_L2, 2023.
[55] Earth engine data catalog search USGS Landsat 8 level 2. https://developers.google.com/earth-engine/datasets/catalog/LANDSAT_LC08_C02_T1_L2, 2023.
[56] Earth engine data catalog search USGS Landsat 7 level 2. https://developers.google.com/earth-engine/datasets/catalog/LANDSAT_LE07_C02_T1_L2, 2023.
[57] US Geological Survey Landsat Missions, 2020. https://www.usgs.gov/core-science-systems/nli/landsat/landsat-7?qt-science_support_page_related_con=0#qt-science_support_page_related_con.
[58] D. Elefftheriou, K. Kiachidis, G. Kalmintzis, A. Kalea, C. Bantasis, P. Koumadoraki, M.E. Spathara, A. Tsolaki, M.I. Tzampazidou, A. Gemitzi, Determination of annual and seasonal daytime and nighttime trends of MODIS LST over Greece - climate change implications, Sci. Total Environ. 616–617 (2018) 937–947, https://doi.org/10.1016/j.scitotenv.2017.10.226.
[59] T. Phan, M. Kappas, T. Tran, Land surface temperature variation due to changes in elevation in northwest vietnam, Climate 6 (2018) 28, https://doi.org/10.3390/cli6020028.
[60] M. Shirgholami, S.A. Masoodian, Assessment of spatial and temporal variations of land surface temperature (LST) due to elevation changes in Yazd Province, Iran, Arabian J. Geosci. 15 (2022) 1372, https://doi.org/10.1007/s12517-022-09943-1.
[61] S. Wafi, M.R. Ismail, The Relationship between thermal performance, thermal comfort and occupants, J. Sustain. Dev. (2008) 675–690.
[62] E.A. Njoku, D.E. Tenenbaum, Quantitative assessment of the relationship between land use/land cover (LULC), topographic elevation and land surface temperature (LST) in Ilorin, Nigeria, Remote Sens. Appl. Soc. Environ. 27 (2022), 100780, https://doi.org/10.1016/j.rsase.2022.100780.
[63] J.D. Lundquist, N. Pepin, C. Rochford, Automated algorithm for mapping regions of cold-air pooling in complex terrain, J. Geophys. Res. 113 (2008), D22107, https://doi.org/10.1029/2008JD009879.
[64] R. Van De Kerchove, S. Lhermitte, S. Veraverbeke, R. Goossens, Spatio-temporal variability in remotely sensed land surface temperature, and its relationship with physiographic variables in the Russian Altay Mountains, Int. J. Appl. Earth Obs. Geoinf. 20 (2013) 4–19, https://doi.org/10.1016/j.jag.2011.09.007.
[65] Y. Vitasse, G. Klein, J.W. Kirchner, M. Rebetez, Intensity, frequency and spatial configuration of winter temperature inversions in the closed La Brevine valley, Switzerland, Theor. Appl. Climatol. 130 (2017) 1073–1083, https://doi.org/10.1007/s00704-016-1944-1.
[66] X. Feng, S. Wang, J. Guo, Temperature inversions in the lower troposphere over the Sichuan Basin, China: seasonal feature and relation with regional atmospheric circulations, Atmos. Res. 271 (2022), 106097, https://doi.org/10.1016/j.atmosres.2022.106097.
[67] T.R. Parish, MOUNTAIN METEOROLOGY | katabatic winds, in: Encyclopedia of Atmospheric Sciences, Elsevier, 2015, pp. 75–79.
[68] F.J. Kruger, D.T. Mitchell, J.U.M. Jarvis, in: F.J. Kruger, D.T. Mitchell, J.U.M. Jarvis (Eds.), Mediterranean-Type Ecosystems, Ecological Studies, 43, Springer Berlin Heidelberg, Berlin, Heidelberg, 1983.
[69] P. Kramer, J. Boyer, Water Relations of Plants and Soils, first ed., 1995.
[70] P.C. Withers, C.E. Cooper, Dormancy, in: Encyclopedia of Ecology, Elsevier, 2008, pp. 952–957.
[71] A. Barat, S. Kumar, P. Kumar, P. Parth Sarthi, Characteristics of surface urban heat island (SUHI) over the gangetic plain of Bihar, India, Asia-Pacific J. Atmos. Sci. 54 (2018) 205–214, https://doi.org/10.1007/s13143-018-0004-4.
[72] H.S. Sussman, A. Raghavendra, L. Zhou, Impacts of increased urbanization on surface temperature, vegetation, and aerosols over Bengaluru, India, Remote Sens. Appl. Soc. Environ. 16 (2019), 100261, https://doi.org/10.1016/j.rsase.2019.100261.
[73] A. Mathew, S. Khandelwal, N. Kaul, Investigating spatial and seasonal variations of urban heat island effect over Jaipur city and its relationship with vegetation, urbanization and elevation parameters, Sustain. Cities Soc. 35 (2017) 157–177, https://doi.org/10.1016/j.scs.2017.07.013.
[74] K. Wang, S. Jiang, J. Wang, C. Zhou, X. Wang, X. Lee, Comparing the diurnal and seasonal variabilities of atmospheric and surface urban heat islands based on the Beijing urban meteorological network, J. Geophys. Res. 122 (2017) 2131–2154, https://doi.org/10.1002/2016JD025304.
[75] C.J. Tomlinson, L. Chapman, J.E. Thornes, C. Baker, Remote sensing land surface temperature for meteorology and climatology: a review, Meteorol. Appl. 18 (2011) 296–306, https://doi.org/10.1002/met.287.
[76] J.E. Nichol, W.Y. Fung, K. Lam, M.S. Wong, Urban heat island diagnosis using ASTER satellite images and 'in situ' air temperature, Atmos. Res. 94 (2009) 276–284, https://doi.org/10.1016/j.atmosres.2009.06.011.
[77] W. Zhou, G. Huang, M.L. Cadenasso, Does spatial configuration matter? Understanding the effects of land cover pattern on land surface temperature in urban landscapes, Landsc. Urban Plann. 102 (2011) 54–63, https://doi.org/10.1016/j.landurbplan.2011.03.009.
[78] M.E. Hereher, Estimation of monthly surface air temperatures from MODIS LST time series data: application to the deserts in the Sultanate of Oman, Environ. Monit. Assess. 191 (2019) 592, https://doi.org/10.1007/s10661-019-7771-y.
[79] J.C. Price, Assessment of the urban heat island effect through the use of satellite data, Mon. Weather Rev. 107 (1979) 1554–1557, https://doi.org/10.1175/1520-0493(1979)107<1554:AOTUHI>2.0.CO;2.
[80] E. Ben-Dor, H. Saaroni, Airborne video thermal radiometry as a tool for monitoring microscale structures of the urban heat island, Int. J. Rem. Sens. 18 (1997) 3039–3053, https://doi.org/10.1080/014311697217198.
[81] E. Soto-Estrada, S. Correa-Echeveri, M.I. Posada-Posada, Thermal analysis of urban environments in Medellin, Colombia, using an unmanned aerial vehicle (UAV), J. Urban Environ. Eng. 11 (2017) 142–149, https://doi.org/10.4090/juee.2017.v11n2.142149.